



Multiple damage detection on aircraft composite structures using near-field MUSIC algorithm



Yongteng Zhong, Shenfang Yuan*, Lei Qiu

The State Key Laboratory of Mechanics and Control of Mechanical Structures, Nanjing University of Aeronautics and Astronautics, No. 29 Yuda Street, Nanjing 210016, PR China

ARTICLE INFO

Article history:

Received 10 October 2013

Received in revised form 17 April 2014

Accepted 19 April 2014

Available online 9 May 2014

Keywords:

Multiple damages

2D-MUSIC

Near-field

Composite structure

ABSTRACT

Damages in composite structure can lead to significant reduction in local strengths. Therefore, it is important to localize these damages to give an early warning for maintenance of the aircraft. Since these damages may happen near the sensor array, the wave fronts are spherical and the far-field multiple signal classification (MUSIC) based methods with the plane wave hypothesis are no longer valid. Aimed at developing MUSIC algorithm to detect near-field damages, a new near-field 2D-MUSIC method using piezoelectric sensor array is presented first. Though ordinary MUSIC algorithms can be used to distinguish multiple sources, they request the signals from these sources are independent with each other. By using the active damage monitoring method, since all damage scattered signals are the damage reflection signals of the same active excitation one, they are all correlated. This gives rise to the difficulty to apply ordinary MUSIC methods to detect multiple damages in the structure using active monitoring approach. To distinguish multiple damages in the structure, a correlated near-field 2D-MUSIC method based on spatial smoothing algorithm is also proposed to solve the correlation problem of multiple damage detection. To verify the proposed methods, evaluation experiments are performed on a carbon fiber composite material plate and a real aircraft composite oil tank. The results prove the effectiveness of the presented methods to detect multiple damages on the complex composite structure.

© 2014 Elsevier B.V. All rights reserved.

1. Introduction

Composite structures have been increasingly used in various aircraft structures due to their superior characteristics. However, the performance and behavior characteristics of in-service composite structures can be affected by damage resulting from external conditions such as impact, and loading abrasion. Therefore, the timely and accurate detection of structural damages are of a major concern in the application of composite structures [1–3].

The guided Lamb wave is widely acknowledged as one of the promising tools for quantitative identification of damage in composite structures [4]. Some representative algorithms include system modeling [5–7], time reversal [8,9] and damage imaging algorithms [10,11].

Recently, sensor array signal processing based methods have emerged to be a set of new interesting structural health monitoring (SHM) methods. Several methods have been reported using the compact sensor arrangement, such as ultrasonic phased arrays

technology [12], directional piezoelectric spatial filter technology [13,14], and subspace approach based MUSIC algorithm for detecting structural damage. Among them, the MUSIC algorithm based method is a new promising method. This algorithm belongs to eigen-structure and sub-space approach which can provide asymptotically unbiased estimation of a general set of signal parameters [15] and can effectively extract key features and successfully detect the source under low signal-to-noise ratio [16]. Several researchers have considered applying MUSIC algorithm for structural health monitoring. Stepinski presented a MUSIC algorithm to estimate the direction of arrival (DOA) of the elastic waves on an aluminum plate using a uniform circular array [17]. Lee employed the MUSIC method to estimate the DOA of impacts on an aluminum plate [18]. However, all the reports are restricted to localize the source under far-field condition. In this case, the waves from the source can be regarded as planar waves received by the sensor array, which can help to reduce the difficulty in estimating the location of the wave source. In real engineering applications, damages may happen near the sensors which are near-field case. In this near-field situation, the wave fronts of the elastic waves can only be considered as spherical other than planar. If the far-field estimation algorithms are still adopted, errors will certainly be big. To deal with

* Corresponding author.

E-mail address: ysf@nuaa.edu.cn (S. Yuan).

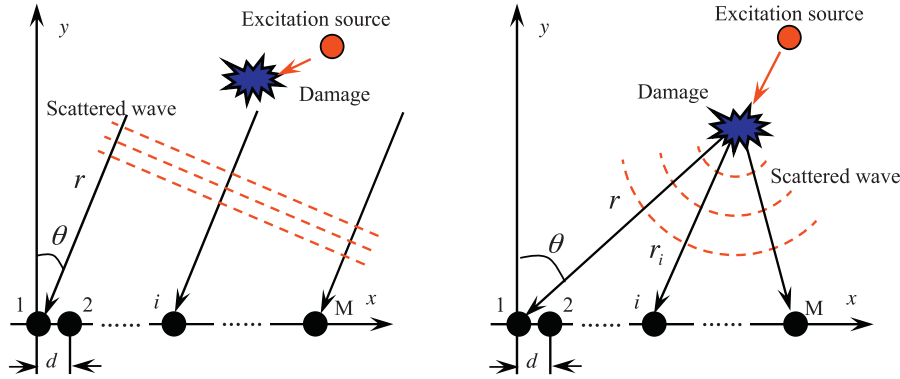


Fig. 1. Damage scattered signal model: (a) far-field case and (b) near-field case.

the near-field monitoring problem and take advantage of the sensor array signal processing, this paper proposes a near-field 2D-MUSIC algorithm first for damage detection of composite structures.

On the other hand, one advantage of the MUSIC algorithm is its ability to detect multiple sources. The multiple source localization ability of MUSIC algorithms has been applied in many engineering areas, such as radar and communication. However, there is no approach reported to apply this method to deal with multiple damages localization in structural health monitoring. This is because ordinary MUSIC algorithm can only work when the sources are independent. The scattered signals induced by multiple damages all come from the inferences of the damages and the same active excitation signal from one PZT sensor in the sensor array when active monitoring approach is adopted. They are all correlated; hence, the ordinary MUSIC algorithm cannot work under this situation. To solve this problem, a novel correlated 2D-MUSIC multiple damages detection method based on spatial smoothing is presented to deal with the multiple damage detection in this paper.

The layout of this paper is as follows: Section 2 presents the near-field MUSIC algorithm for damage detection. The correlated 2D-MUSIC detection method based on spatial smoothing is proposed in Section 3 for multiple damage detection. In Section 4, validation experiments are performed to verify the proposed method on a carbon fiber composite plate and a real aircraft composite oil tank. Discussion is also given in the section regarding the evaluation results.

2. Near-field MUSIC algorithm for damage detection

The Lamb wave-based damage detecting techniques use a two-stage prediction model to find the difference in the signals between defective structure and benchmark which is very suitable for monitoring the propagation of damages [19]. In this active research, the difference signals known as scattered waves are analyzed for damage detection.

2.1. Far-field case

The far-field damage case is analyzed first. Then it is expanded to the near-field situation. As seen in Fig. 1, a uniform linear sensor array (ULSA) consisting of M piezoelectric (PZT) sensors is arranged on the structure. The distance between two sensors is d . The length of the sensor array is L , where $L = (M - 1)d$. To ensure the approximation condition in the analysis, d has to be small enough to meet the condition of $d \leq \lambda/2$, where λ is the wavelength of wave signal [20]. As seen in Fig. 1(a), the wave fronts arriving at the sensor array can be considered as planar. θ denotes the wave propagating direction with respect to the coordinate y axis. r is defined as the distance between the damage source and the ULSA which is the

distance from the source to the reference sensor labeled 1 in the sensor array.

Let $\mathbf{x}_i(t)$ denote the output from PZTi of the sensor array observed at time t , it can be expressed as

$$\mathbf{x}_i(t) = \mathbf{s}_i(t) + \mathbf{n}_i(t), \quad i = 1, 2, \dots, M \quad (1)$$

where $\mathbf{n}_i(t)$ is the output corresponding to the background noise.

Considering the scattered waves with a certain frequency component of ω_0 arriving at the sensor array, the corresponding output $\mathbf{s}_1(t)$ from PZT1 can be represented by Eq. (2)

$$\mathbf{s}_1(t) = u(t)e^{j(\omega_0 t - kr)} \quad (2)$$

where $u(t)$ is the signal output amplitude, $k = \omega_0/c$ is the wavenumber. In this case of ULSA, the difference of propagation distance from the damage source to the reference PZT1 and PZTi $\Delta r_i = (i - 1)d \sin \theta$, and the output from PZTi can be represented as

$$\mathbf{s}_i(t) = u_i(t)e^{j[\omega_0 t - k[r - (i - 1)d \sin \theta]]} = u_i(t)e^{j(\omega_0 t - kr)}e^{j\omega_0 \frac{(i-1)d \sin \theta}{c}} \quad (3)$$

Define τ_i is the arriving time difference between PZTi and PZT1, which is

$$\tau_i = \frac{(i - 1)d \sin \theta}{c} \quad (4)$$

Define $\mathbf{s}_i(t) = \mathbf{s}(t - \tau_i)$ and $u_i(t) = u(t - \tau_i)$, Eq. (2) can be rewritten as Eq. (5)

$$s(t - \tau_i) = u(t - \tau_i)e^{j(\omega_0 t - kr)}e^{j\omega_0 \tau_i}. \quad (5)$$

Under the far-field assumption, since $d \leq \lambda/2$, the time difference $\tau_i \propto 1/f$ has only several orders of magnitude of the reciprocal of the frequency. Therefore, the amplitude output by different sensors in the array can be thought to be the same, shown by Eq. (6)

$$u(t - \tau_i) \approx u(t). \quad (6)$$

By substituting Eqs. (2) and (6) into Eq. (5), Eq. (5) can be rewritten as Eq. (7)

$$s_i(t) \approx s(t)e^{j\omega_0 \tau_i}. \quad (7)$$

By substituting Eq. (7) into Eq. (1), Eq. (8) is obtained as

$$x_i(t) = s(t)e^{j\omega_0 \tau_i} + n_i(t), \quad i = 1, 2, \dots, M. \quad (8)$$

Define $a_i(\theta)$ as the array steering vector for the scattered signal which can be represented as

$$a_i(\theta) = \exp(j\omega_0 \tau_i). \quad (9)$$

The observed signal vector of the array with M PZT sensors under far-field situation can be represented as

$$\mathbf{X}(t) = \mathbf{A}(\theta)s(t) + \mathbf{N}(t) \quad (10)$$

Table 1

Mechanical parameter of single layer of the carbon fiber composite structure.

0° tensile modulus (GPa), E_{11}	90° tensile modulus (GPa), E_{22}	$\pm 90^\circ$ in-plane shearing modulus (GPa), E_{22}	Main Poisson ratio	Density (kg m^{-3})
135	8.8	4.47	0.328	1.61×10^3

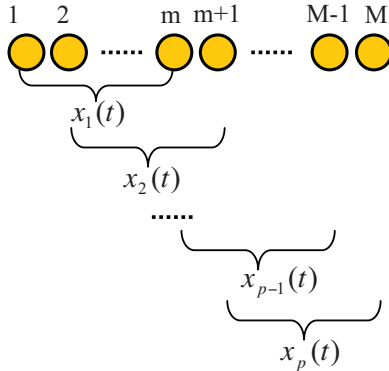


Fig. 2. Forward spatial smoothing algorithm.

where

$$\mathbf{X}(t) = [x_1(t), x_2(t), \dots, x_M(t)]^T$$

$$\mathbf{A}(\theta) = [\mathbf{a}_1(\theta), \mathbf{a}_2(\theta), \dots, \mathbf{a}_k(\theta)]^T$$

$$\mathbf{s}(t) = [\mathbf{s}_1(t), \mathbf{s}_2(t), \dots, \mathbf{s}_k(t)]^T$$

$$\mathbf{N}(t) = [\mathbf{n}_1(t), \mathbf{n}_2(t), \dots, \mathbf{n}_M(t)]^T$$

2.2. Near-field case

When the distance between the ULSA and the source is small enough to meet Eq. (11), the monitoring case has to be considered as a near-field monitoring case [20].

$$r_{\text{near}} \leq \frac{2L^2}{\lambda} \quad (11)$$

Fig. 1(b) shows the near-field situation. Since the wave source is close to ULSA, the wave fronts are circle and cannot be considered to be planar anymore. θ denotes the wave propagating direction caused by damage with respect to the coordinate x axis. r_i denotes the distance from the damage to the PZTi respectively.

Under the near-field situation, the distance from the damage source to each sensor has big difference which cannot be neglected anymore. To simplify the calculation and considering the near-field situation, the amplitude attenuation is approximated as linear attenuation.

$$u(t - \tau_i) \approx \frac{r_1}{r_i} u(t) \quad (12)$$

As seen in Fig. 1(b), a triangle composed of PZT1, PZTi and damage source which is used to calculate the τ_i . The triangle is composed of the distance r_1 between damage source and PZT1, the distance r_i between damage source and PZTi, the distance $(i-1)d$ between PZT1 and PZTi. τ_i should be expressed as

$$\tau_i = \frac{r_1 - r_i}{c} \quad (13)$$

According to this triangle, r_i can be obtained by cosine theorem

$$r_i = \sqrt{r_1^2 + (i-1)^2 d^2 - 2r_1(i-1)d \cos(90^\circ - \theta)} \quad (14)$$

thus,

$$\tau_i = \frac{r_1 - \sqrt{r_1^2 + (i-1)^2 d^2 - 2r_1(i-1)d \sin \theta}}{c}. \quad (15)$$

To simplify the calculation, τ_i is represented by its second-order Taylor expansion about τ_1 as shown by Eq. (16)

$$\tau_i = \frac{\tau'(i)|_{i=1}}{1!}(i-1) + \frac{\tau''(i)|_{i=1}}{2!}(i-1)^2 + O((i-1)^2). \quad (16)$$

By calculating the first derivative $\tau'(i)|_{i=1}$ and second derivative $\tau''(i)|_{i=1}$, Eq. (17) can be obtained

$$\tau_i = \frac{(-d \sin \theta)}{c}(i-1) + \left(-\frac{d^2}{cr_1} \cos^2 \theta \right)(i-1)^2 + O\left(\frac{d^2}{r_1^2}\right) \quad (17)$$

By substituting Eqs. (12) and (17) into Eq. (7), the observed data output from PZTi under the near-field situation can be represented as Eq. (18)

$$\mathbf{x}_i(t) = \frac{r_1}{r_i} \mathbf{s}(t) e^{j\omega_0 \tau_i} + \mathbf{n}_i(t), \quad i = 1, 2, \dots, M \quad (18)$$

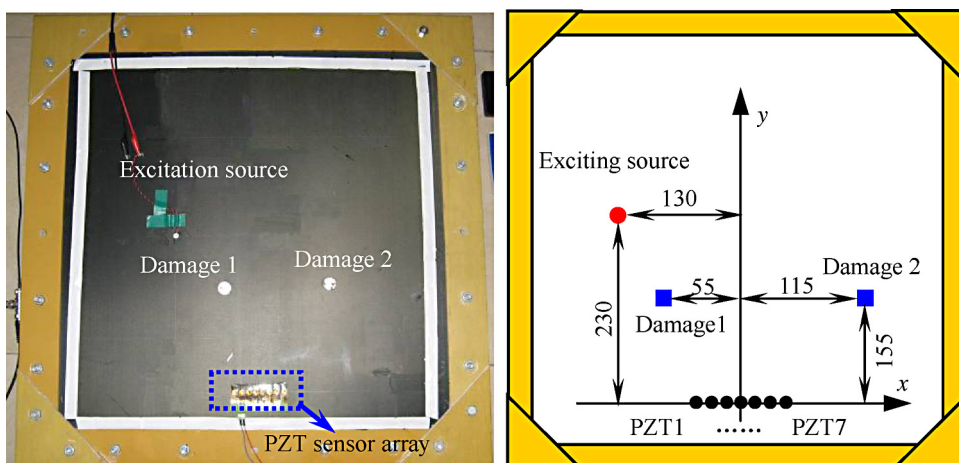


Fig. 3. The carbon fiber plate and simulation damage position (mm).

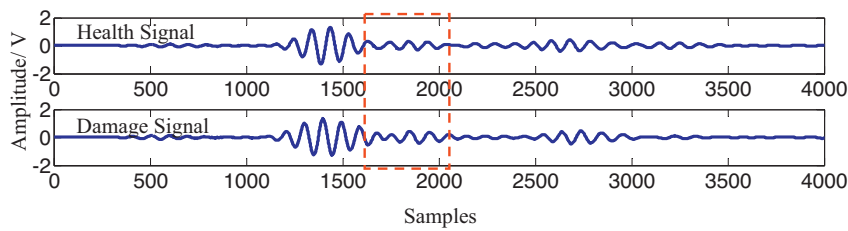


Fig. 4. Comparison of the time domain signal between the health and damage of PZT1.

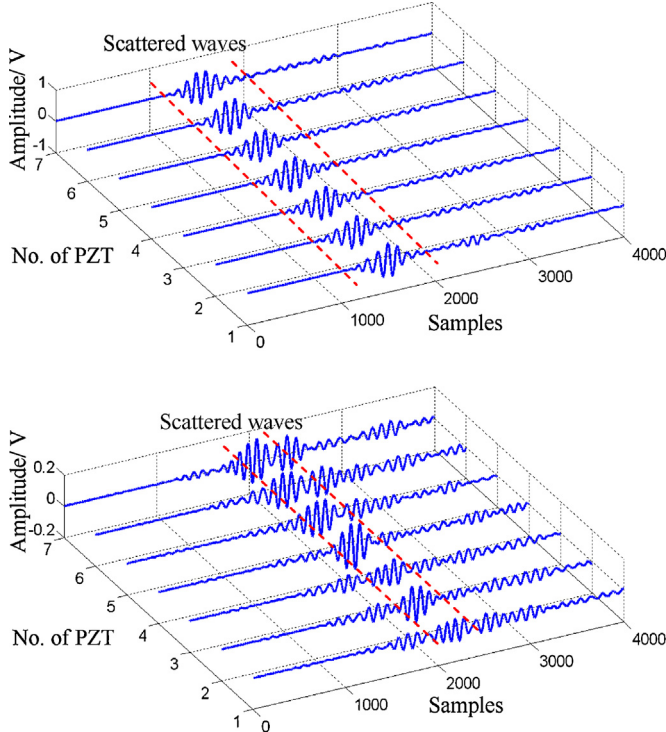


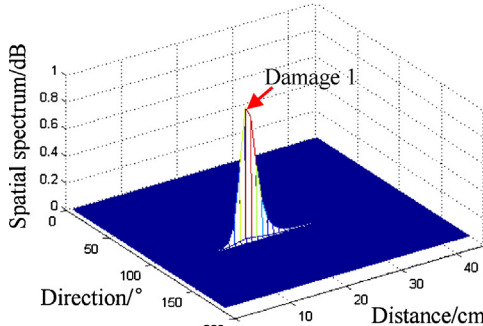
Fig. 5. The waterfall plot of the scattered signals of single damage of carbon fiber composite plate: (a) damage 1 and (b) damage 2.

The array steering vector for the scattered signal is

$$a_i(r, \theta) = \frac{r_1}{r_i} \exp(j\omega_0 \tau_i) \quad (19)$$

For the whole sensor array, the observed input signal vector can be represented as

$$\mathbf{X}(t) = \mathbf{A}(r, \theta)\mathbf{s}(t) + \mathbf{N}(t) \quad (20)$$



where

$$\mathbf{X}(t) = [x_1(t), x_2(t), \dots, x_M(t)]^T$$

$$\mathbf{A}(r, \theta) = [a_1(r, \theta), a_2(r, \theta), \dots, a_k(r, \theta)]^T$$

$$\mathbf{s}(t) = [s_1(t), s_2(t), \dots, s_k(t)]^T$$

$$\mathbf{N}(t) = [n_1(t), n_2(t), \dots, n_M(t)]^T$$

The covariance matrix of the observed signal vector from the sensor array is

$$\begin{aligned} \mathbf{R} = E[\mathbf{XX}^H] &= AE[ss^H]A^H + AE[sN^H] + E[sN^H]A^H \\ &\quad + E[NN^H]. \end{aligned} \quad (21)$$

$E[\cdot]$ denotes covariance computation, and the superscript H denotes the complex conjugate transpose. Assuming that signal and noise are independent and the background noise is Gaussian white, Eq. (21) can be simplified as

$$\mathbf{R} = \mathbf{A}\mathbf{R}_S\mathbf{A}^H + \sigma^2\mathbf{I} \quad (22)$$

where \mathbf{R}_S is the covariance matrix of signal, and σ^2 is noise power. \mathbf{I} denotes the covariance matrix of noise. Because noise arriving at the sensor array is of equal power and uncorrelated, \mathbf{I} stands for $M \times M$ identity matrix.

If the source signal is stronger than the noise signals and they are uncorrelated, according to the classical MUSIC algorithm [15], the covariance matrix can be decomposed into two parts, including a signal-related part and a noise-related part.

The eigenvalue decomposition of \mathbf{R} is

$$\mathbf{R} = \mathbf{U}_S \sum_S U_S^H + \mathbf{U}_N \sum_N U_N^H. \quad (23)$$

Here, the subscript "S" and "N" are short name of "source" and "noise", and denote the signal subspace and noise subspace respectively. \mathbf{U}_S denotes the signal subspace spanned by the eigenvector matrix corresponding to the largest eigenvalue. \mathbf{U}_N denotes the noise subspace spanned by the eigenvector matrix corresponding to those small eigenvalues.

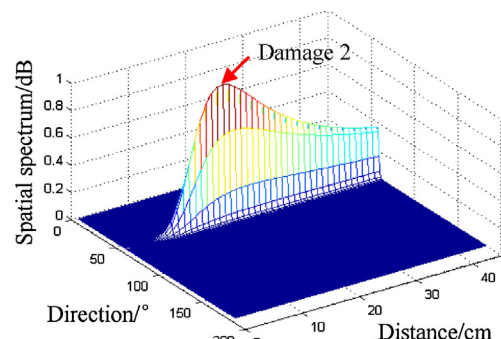


Fig. 6. The spatial spectrum estimated by near-field MUSIC: (a) damage 1 and (b) damage 2.

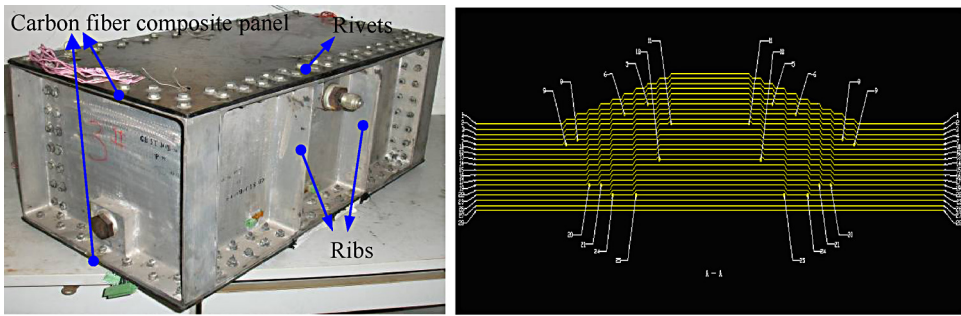


Fig. 7. (a) Aircraft oil tank composite structure and (b) the carbon fiber composite plate with varied thickness.

Assuming that \mathbf{D} signals are independent, the eigenvalue subspace has the following properties:

a. The signal subspace \mathbf{U}_S spanned by the eigenvector matrix corresponding to the D largest eigenvalue and the subspace spanned by the steering vector are in the same space, which is

$$\text{span}\{e_1, e_2, \dots, e_D\} = \text{span}\{a_1, a_2, \dots, a_D\}. \quad (24)$$

b. The other eigenvectors $\text{span}\{e_{D+1}, \dots, e_M\}$ become the basis of the orthogonal complement of the signal subspace, and the subspace spanned is termed noise subspace.

c. When the background noise is Gaussian white, the signal subspace \mathbf{U}_S and the noise subspace \mathbf{U}_N are orthogonal

$$\mathbf{A}^H \mathbf{U}_N = 0. \quad (25)$$

Since that the ideal covariance matrices \mathbf{R} is unknown, it is estimated by using a finite number of data vectors. $\hat{\mathbf{R}}$ is the estimation of \mathbf{R} which can be calculated by Eq. (26)

$$\hat{\mathbf{R}} = \frac{1}{N} \mathbf{X} \mathbf{X}^H \quad (26)$$

where $\mathbf{X} = [X(1), X(2), \dots, X(N)]$, N is the number of the snapshots.

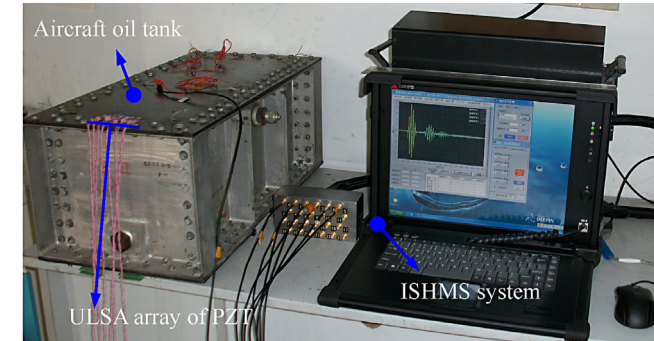


Fig. 8. Experiment setup and the sensors array layout diagram (mm).

To describe the orthogonal properties described above, the spatial spectrum is used which can be calculated by Eq. (27)

$$\mathbf{P}_{\text{MUSIC}}(r, \theta) = \frac{1}{\mathbf{A}^H(r, \theta) \mathbf{U}_N \mathbf{U}_N^H \mathbf{A}(r, \theta)} \quad (27)$$

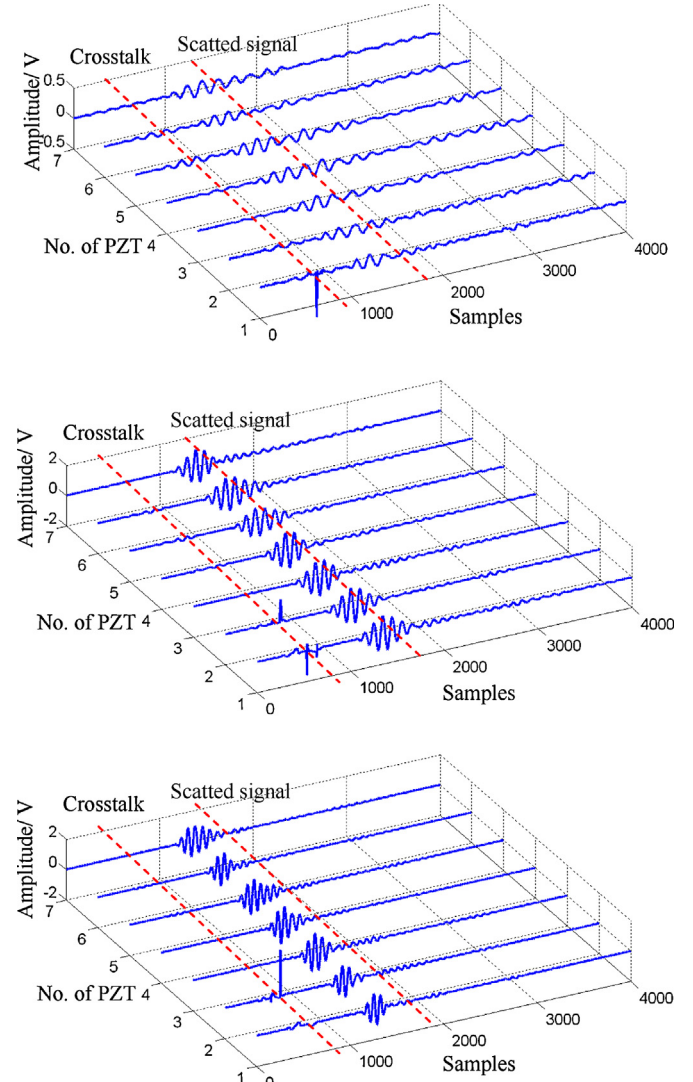


Fig. 9. The waterfall plot of the scattered signals of single damage at different exciting frequencies: (a) 30 kHz, (b) 50 kHz, and (c) 70 kHz.

Table 2

The results of damages estimation and relative errors.

Damage case	Parameters		Predictive position		Errors	
	Actual position r/mm	$\theta/^\circ$	\hat{r}/mm	$\hat{\theta}^\circ$	E_r/mm	$E_\theta/^\circ$
1	164.4	109.5	161	107	3.4	1.5
2	193	53.4	180	56	13	2.6

Table 3

Simulated damage positions.

Damage case							
1	2	3	4	5	6		
r/mm	125	131	132	113	125	131	122
$\theta/^\circ$	90	108	70	131	90	108	71

where

$$A(r, \theta) = \begin{bmatrix} 1 \\ \vdots \\ \frac{r_1}{r_i} \exp \left(-j \left(-\frac{2\pi fd}{c} \sin \theta \right) (i-1) + \left(-\frac{\pi fd^2}{cr_1} \cos^2 \theta \right) (i-1)^2 \right) \\ \vdots \\ \frac{r_1}{r_M} \exp \left(-j \left(-\frac{2\pi fd}{c} \sin \theta \right) (M-1) + \left(-\frac{\pi fd^2}{cr_1} \cos^2 \theta \right) (M-1)^2 \right) \end{bmatrix}.$$

Based on Eq. (27), by varying r and θ to realize a scanning process, $A(r, \theta)$ is steered to scan the whole structure area. The peak point on the spatial spectrum corresponds to the damage source point. Both the distance and direction of the source can be obtained.

3. The correlated 2D-MUSIC detection method based on spatial smoothing

Considering the special case where the two sources are completely coherent with each other, the rank of covariance matrix rank will reduce which results that the dimension of signal space is less than the number of damage sources. The steering vector and the noise subspace could not be completely orthogonal of Eq. (25). Hence, the core problem of estimating signal source direction correctly when the sources are correlated is how to restore the rank of covariance matrix.

Table 4

Single simulated damage detection results.

Damage case	Parameters		Predictive positions		Predicted error	
	Actual positions		Predictive positions		E_r	E_θ
	r/mm	$\theta/^\circ$	\hat{r}/mm	$\hat{\theta}^\circ$		
1	125	90	125	91	0	1
2	131	108	122	107	9	1
3	132	70	122	71	10	1
4	113	131	100	128	13	3

Table 5

Multiple simulated damages detection results.

Damage case	Parameters		Predictive positions				Predicted error					
	Actual positions				Predictive positions				E_r^1	E_θ^1	E_r^2	E_θ^2
	r_1	θ_1	r_2	θ_2	\hat{r}_1	$\hat{\theta}_1$	\hat{r}_2	$\hat{\theta}_2$				
5	125	90	131	108	100	91	130	107	25	1	1	1
6	122	71	131	108	98	72	150	109	24	2	19	1

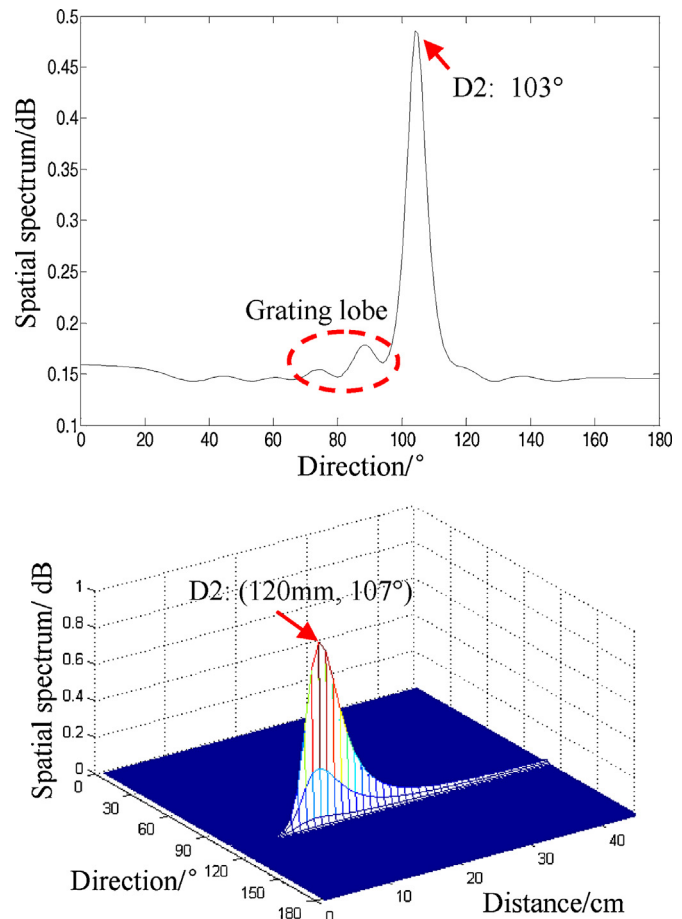


Fig. 10. The spatial spectrum estimated of simulated damage D2 (a) far-field MUSIC and (b) near-field MUSIC.

The spatial smooth techniques have been applied in acoustics, radar and navigation areas for estimate the interference parameters [21–23]. It has been proved that the smoothed covariance matrix is nonsingular and exactly the same form as the covariance matrix for an uncorrelated case if the number of subarrays is greater than the number of signals. To solve the correlation problem of active approach in structural health monitoring area, the spatial

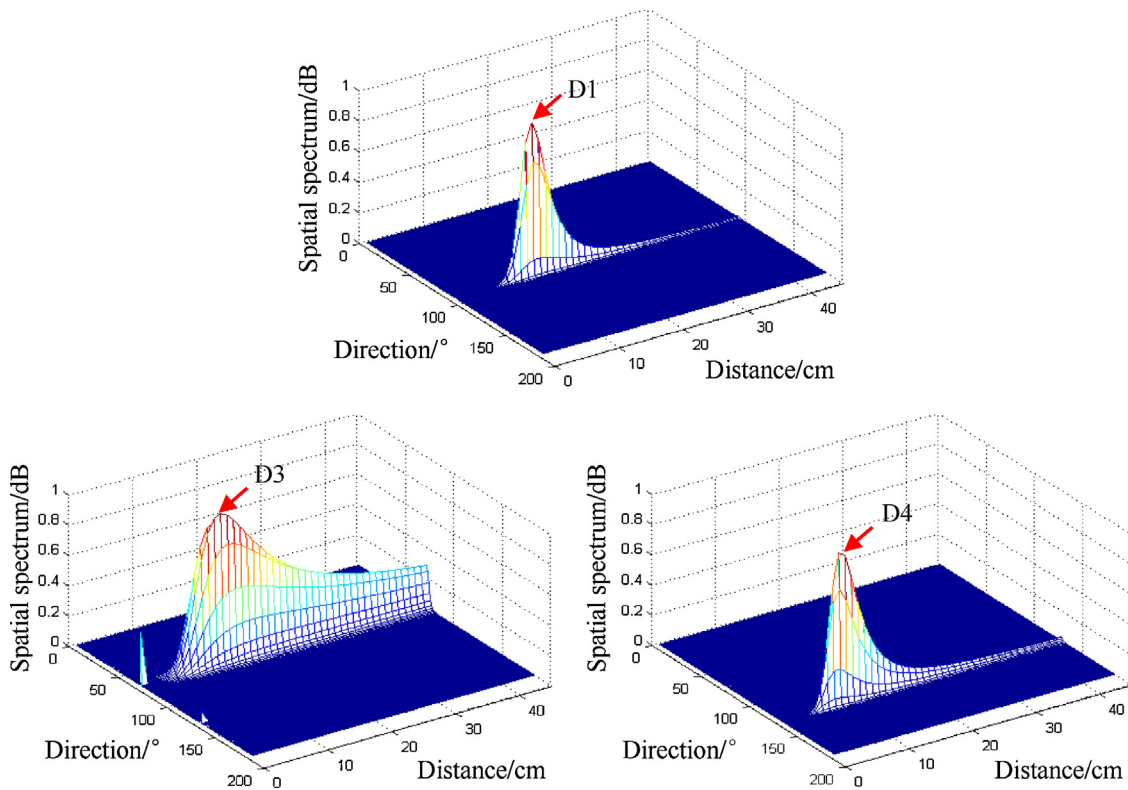


Fig. 11. The spatial spectrum estimated by near-field MUSIC of simulated damage.

smoothing algorithm is presented for multiple damage detection in composite structures.

By using the spatial smoothing method, the total sensor array is separated into several subarrays. The covariance matrices of the subarrays are averaged to get a smoothed covariance matrix. As seen in Fig. 2, the uniform linear array with M PZT sensors can be split into p overlapping subarrays, and each subarray comprises of m PZT sensors.

Defining the following transition matrix Z_k

$$Z_k = [0_{m \times (k-1)} | I_{m \times m} | 0_{m \times (p-k)}]. \quad (28)$$

The first subarray is defined as reference subarray element, and let $\mathbf{x}_k(t)$ denote the output from the k th subarray observed at time t , it can be expressed as

$$\mathbf{x}_k(t) = [x_k, x_{k+1}, \dots, x_{k+m-1}] = x Z_k X(t). \quad (29)$$

Therefore, the covariance matrix of signal $\mathbf{x}_k(t)$ is

$$R_k = Z_k \hat{R} Z_k^H. \quad (30)$$

And the forward-smoothed source covariance matrix R^f can be obtained as

$$R^f = \frac{1}{p} \sum_{i=1}^p R_k = \frac{1}{p} Z_k \hat{R} Z_k^H. \quad (31)$$

4. Experiment investigation

4.1. Evaluation on carbon fiber composite plate

4.1.1. Experimental setup

The experiment is firstly conducted on a uniform carbon fiber composite plate. The dimension of the composite plate is 600 mm × 600 mm × 2 mm. The composite structure is stacked by 18 layers, the thickness of each layer is 0.12 mm and the ply

sequence is [45/0/−45/90/0/−45/0/−45/0]s, and the material property of each layer is shown in Table 1. The array used in the experiment is a ULSA bonded on the structure surface with seven PZT sensors. The diameter of the PZT sensor is 8 mm. These sensors are arranged with a space of 10 mm and are labeled as PZT1 to PZT7 respectively from the left to the right, and one additional actuator placed at the position (−130 mm, 230 mm) is used to introduce the interrogating signal. The sampling rate is set to 5 MHz, the exciting frequency is set to 50 kHz and the sampling length is set to 4000.

4.1.2. Damage signal analysis

The complex Shannon wavelet based phase velocity measuring method proposed by Qiu et al. [24] is used to measure the phase velocity of 50 kHz signal. The measured phase velocity c obtained is 1437 m/s. Then, the wavelength can be calculated as

$$\lambda = \frac{c}{f} = \frac{1437}{50,000} = 28.7 \text{ mm}. \quad (32)$$

Therefore, the sensor spacing $d = 10 \text{ mm} < \lambda/2$. According to Eq. (11), the near-field condition that the distance between the ULSA and damage can be obtained as

$$r_{near} \leq \frac{2L^2}{\lambda} = \frac{2(60)^2}{28.7} = 250.8 \text{ mm}. \quad (33)$$

Delamination is one of types of failure induced by low-velocity impact [25]. An added mass can simulate wave scattering due to changes in local stiffness which would represent that caused by delamination damage [26,27]. Therefore, to reduce the experiment cost, a mass block with 10 mm diameter circular section was bonded on the plate for the validation of the proposed damage localization method. Two different simulated damages located at the position (164.5 mm, 109.5°) and (193 mm, 53.4°), shown in Fig. 3, are investigated, both of them are in the near-field.

The processing scheme of acquired signal in the experiment is: (a) collecting the health signal; (b) adding the damage 1, and

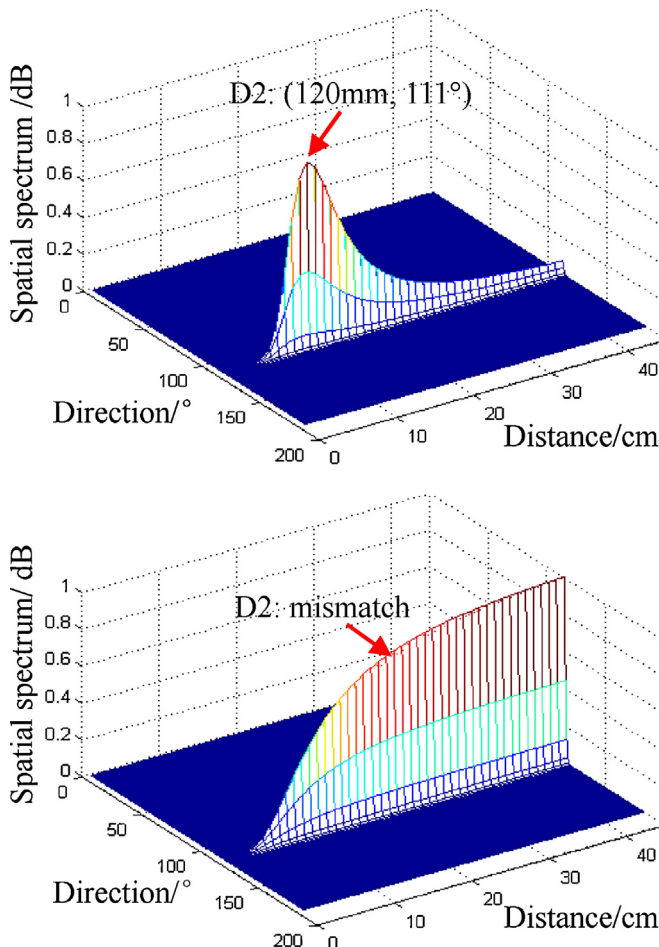


Fig. 12. The spatial spectrum estimated by near-field MUSIC of simulated damage (a) $M=5$ and (b) $M=3$

collecting the damage signal; (c) removing the mass block to the position of damage 2, and collecting the damage signal; and (d) computing the difference signal of the process (b) and (c) respectively as the input vectors of the near-field MUSIC algorithm.

As shown in Fig. 4, the health and damage time domain signal of PZT1 obviously differed in phase and amplitude from 1500 to 2000 samples. Difference signals between the health and damage signal are adopted here in order to reduce the effect of the complicated boundary reflection waves and environmental factors. The scattered signals produced by damages 1 and 2 are shown in Fig. 5. As seen in Fig. 5(a), the signal wave fronts of damage 1 obviously appear in the difference signal from 1500 to 2000 sample. Because damage 2 is not located in the direct path from exciting position to PZT sensor array, the amplitude of scattered signal produced by damage 2 is smaller than that of damage 1, and the scattered signal is more complex, where scattered signal fronts ambiguously appear from 2000 to 2500 sample.

4.1.3. Damage localization results

The near-field MUSIC based localization method is employed for simultaneously estimating the distance and direction of these damages. By scanning interested region, we can obtain the spatial spectrum $P(r, \theta)$ shown in Fig. 6, which represents spatial spectrum magnitudes of each scanned point (r, θ) , and where the peak of the figure represents the damage point localized by the presented 2D-MUSIC algorithm. Comparing the spatial spectrum in two figures, the spectrum peak in Fig. 6(a) is more “sharp” than that in Fig. 6(b). The phenomena of the results would be caused by the differences

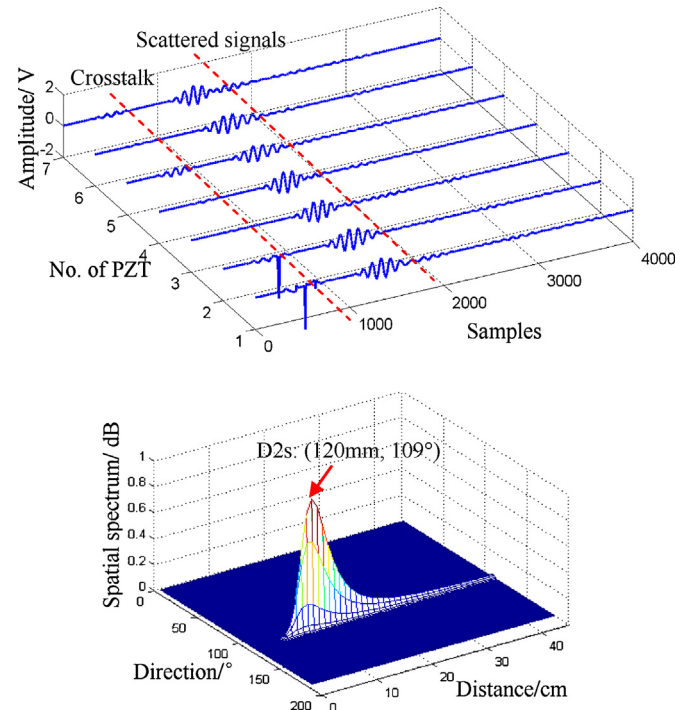


Fig. 13. The waterfall plot of the scattered signals and spatial spectrum estimated by near-field MUSIC of small damage size.

of scattered signal. The predicted damage localization results and errors of the damage parameters are reported in Table 2, which are in good agreement with the actual position. The maximum error in direction estimation is less than 2.6° , and the maximum error in distance estimation is less than 1.3 cm.

4.2. Evaluation on a real composite oil tank

In this section, the proposed method is then applied to a real aircraft composite oil tank. This structure has a dimension of $610\text{ mm} \times 310\text{ mm} \times 240\text{ mm}$. The composite panel is made of T300/QY8911 carbon fiber with a variable thickness, shown in Fig. 7. The thickest part is in the middle of the panel which is 7 mm and the thinnest part is at the two ends with only 4.5 mm thick. The thickness of each layer is 0.125 mm and the ply sequence is [45/0/−45/0/90/0/45/0/−45/0/45/0/0/45/0/−45/0/−45/0/0/45/0/90/0/−45/0/45/0/−45].

4.2.1. Experimental setup

The evaluation setup is shown in Fig. 8. The integrated structural health monitoring scanning system (ISHMS) developed by Qiu

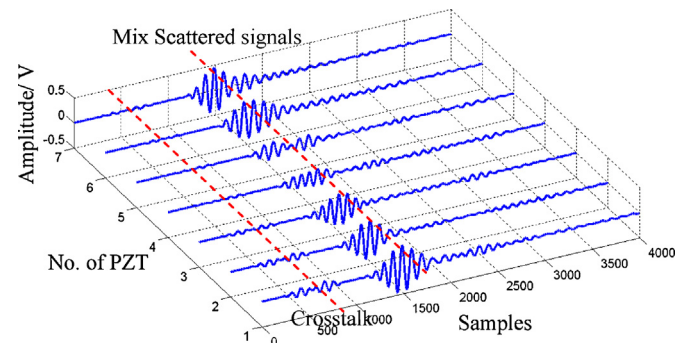


Fig. 14. The waterfall plot of the scattered signals of multiple damages.

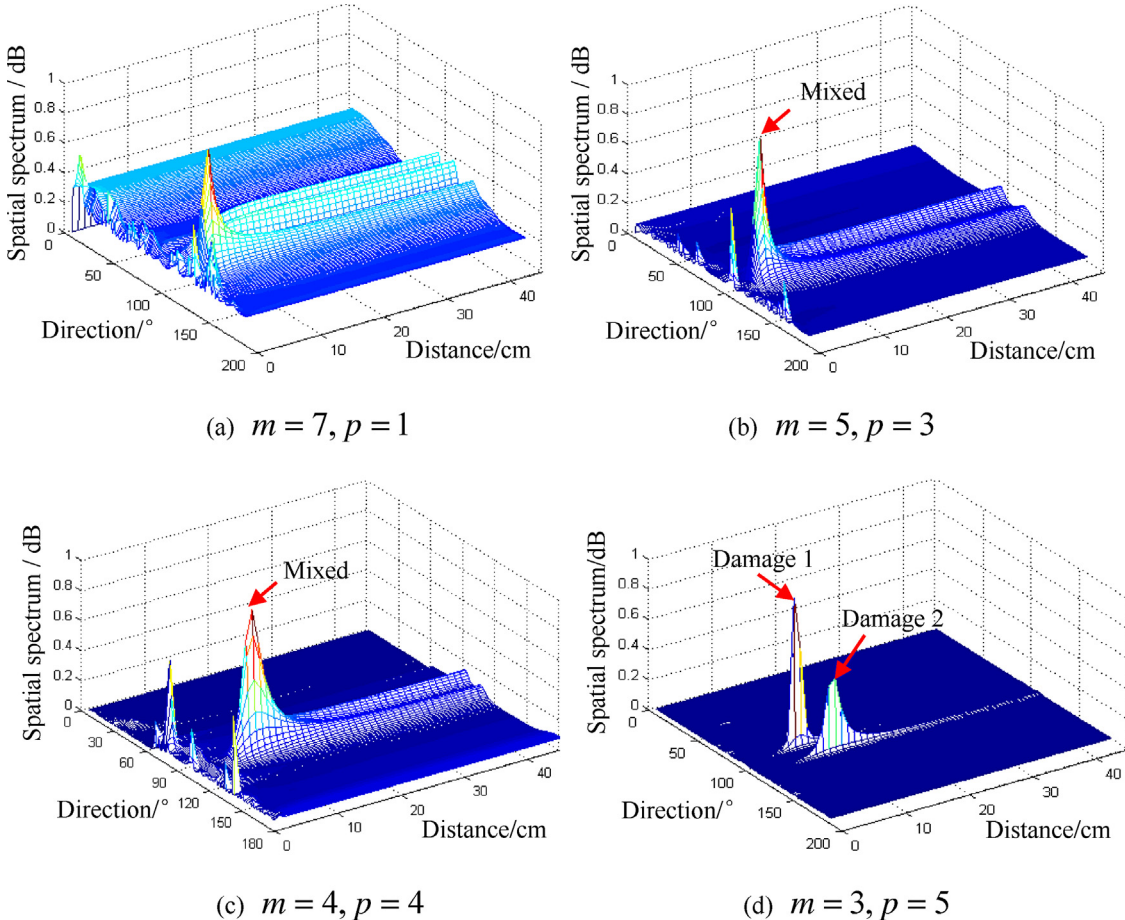


Fig. 15. The spatial spectrum estimated by near-field MUSIC of dual simulated damages.

and Yuan is adopted here as the monitoring equipment [28]. This system is developed to control the excitation and sensing of the PZT sensor array. Fig. 8 shows the ULSA including seven PZT sensors bonded on the structure which are labeled as PZT1, PZT2, ..., PZT7 respectively and one additional actuator element placed at the position (-85 mm , 245 mm) is used to introduce the interrogating signal. The diameter of the PZT sensor is 8 mm and they are arranged with a space of 10 mm .

4.2.2. Damage localization for a single damage

Four simulated damages are placed at different positions seen in Fig. 8 and Table 3. Damage at the position (131 mm , 108°) is chosen as a typical case to be analyzed firstly. In the experiment, the sampling rate is set to 5 MHz and the sampling length is set to 4000 including 500 pre-trigger samples.

4.2.2.1. Exciting frequency selection. When excited signal set to 30 kHz , 50 kHz and 70 kHz arrived at the simulated damage respectively, the scattered signals are produced and the output of sensors array are shown in Fig. 9. As seen in Fig. 9(a), there is very little energy in the scattered signals excited by 30 kHz , and their wave fronts are not seen obviously. Although the wave fronts in the scattered signals excited by 70 kHz could be seen obviously between 1000 and 2000 samples in Fig. 9(c), there are different Lamb modes appearing in each wave. In order to minimize the Lamb wave modes appearing in the wave and strengthen the signal, the exciting frequency is selected as 50 kHz . According to Eqs. (32) and (33), the measured phase velocity c of 50 kHz obtained is 1310 m/s . The calculation wavelength $\lambda = 26.2\text{ mm}$. Therefore, the

spacing $d = 10\text{ mm} < \lambda/2$ satisfied the condition and four simulated damages satisfied the near-field condition.

4.2.2.2. Far-field and near-field localization comparison. To compare the proposed method with the far-field based damage localization method, two methods are used to locate the typical simulated damage. Fig. 10(a) shows the spatial spectrum obtained by far-field MUSIC. The algorithm can only give the direction result where the result of direction estimation is 103° and the error is 5° , and grating lobe shows up at other undesired direction besides the main lobe. Using the near-field MUSIC, the damage occurring direction and distance can be simultaneously found from the spatial spectrum shown in Fig. 10(b). The error of direction estimation is 1° and the error in distance estimation is 1.1 cm . It shows that the near-field MUSIC based method has a high estimation precision, and the far-field MUSIC based method cannot be effective in the near-field situation. Another disadvantage of far-field MUSIC algorithm is that this method cannot estimate the damage distance directly.

Other three simulated damage obtained by near-field MUSIC are shown in Fig. 11, and estimated results of damage points and the errors compared with simulated damage points are listed in Table 4. Four predicted positions of damages are in good agreement with the actual simulated damages location. The maximum error is at the damage position (113 mm , 131°) whose direction and distance error is 3° and 2.1 cm respectively.

4.2.2.3. Number of PZT in the sensor array. Fig. 12(a) and (b) shows the spatial spectrum obtained by near-field MUSIC when the number of PZT is reduced to 5 and 3 respectively. In comparison with

the spatial spectrum in Fig. 10(b), the “spectrum peak” gets larger, and it breaks down when the number of PZT is 3. It shows that the effect of increasing the number of elements can sharpen the main lobe to improve the sensitivity of the proposed method. However, in practice, more elements will result in wiring issue and will be limited by the available installation space. Therefore, there are seven PZT sensors used in the experiment.

4.2.2.4. Effect of damage size. To study the effect of damage size, a simulated damage with a mass block with 5 mm diameter circular section was bonded on the structure. The scattered signals are produced and the output of sensors array is shown in Fig. 13(a). Seen in the figure, the energy in this scattered signal is smaller than that in Fig. 9(b), but its wave fronts can be seen obviously. Fig. 13(b) shows the spatial spectrum obtained is almost the same as Fig. 10(b), whose direction and distance error is 1° and 1.1 cm respectively. It shows that the sensitivity of proposed method depends on the quality of the wave fronts of scattered signal induced by damages, and the damage size is not a direct factor which affects the localization method.

4.2.3. Damage localization for multiple damages

Multiple damages at the position (125 mm, 90°) and (131 mm, 108°) are chosen as a typical case to be analyzed. The output scattered sensors array signals of dual simulated damage sources are shown in Fig. 14. The scattered signals produced by multi-damage mix up cannot be divided in the time-domain signal. Firstly, the 2D-MUSIC algorithm is applied for locating damages. The spatial spectrum figures estimated are shown in Fig. 15(a). From this figure, only one peak exists and other strong and disturbing lobes show up. It shows that the algorithm performance is degraded when the multiple damages are correlated, since the covariance matrix is singular.

According to Section 2.2, the whole PZT sensor array is split into 5, 4 and 3 overlapping subarrays, and each subarray comprises 3, 4 and 5 PZT sensors respectively and the spatial spectrum figures estimated are shown in Fig. 15(b)–(d). Seen as in these figures, the correlated 2D-MUSIC damage method could locate the multiple damages accurately when the whole PZT sensor array is split into five overlapping subarrays, whose maximum direction error is 1° , and the maximum distance error is 2.5 cm. The predicted results of dual simulated damage points and the errors comparing with actual locations are listed in Table 5.

5. Conclusion

This paper investigates a damage detection method based on 2D-MUSIC algorithm and a correlated 2D-MUSIC algorithm using compact PZT sensors array for locating single damage and multiple damages of aircraft composite structure.

The performance of the proposed method is firstly verified on a carbon fiber composite plate. It shows that the far-field MUSIC based method cannot be effective in the near-field situation and the near-field 2D-MUSIC based localization method has a high estimation precision. Two single simulated damage results have shown that the proposed algorithm attains a good performance when the wave velocity can be assumed constant within the structure, whose error in direction estimation is less than 2.6° , and the maximum error in distance estimation is less than 1.3 cm. Then, the proposed method is applied to locate single simulated damage and multiple damages on a real aircraft composite oil tank. Predicted positions are in good agreement with the simulated damages location, and the multiple damages results show that the spatial smoothing based 2D-MUSIC multiple damages detection method is effective in quantifying localized multi-damage in composite structure.

However, further research is still worthy to address systematically the influence of the anisotropy performance of the composite on the proposed method. Besides, detailed research also needs to be performed on real structural damage in future research.

Acknowledgments

This work is supported by National Science Foundation for Distinguished Young Scholars of China (Grant no. 51225502), National Natural Science Foundation for Young Scholars of China (Grant no. 51205189) and the EU-FP7 SICA program (Grant no. FP7-PEOPLE-2010-IRSES-269202).

References

- [1] K.Y.L. Leung, Y.L. Yang, Y. Xu, P. Tong, S.K.L. Lee, Delamination detection in laminate composites with an embedded fiber optical interferometric sensor, *Sens. Actuators A: Phys.* 119 (2005) 336–344.
- [2] J. Moll, R.T. Schulte, B. Hartmann, C.P. Fritzen, O. Nelles, Multi-site damage localization in anisotropic plate-like structures using an active guided wave structural health monitoring system, *Smart Mater. Struct.* 19 (2010) 045022.
- [3] H.Y. Guo, Z.L. Li, Two-stage multi-damage detection method based on energy balance equation, *J. Nondestruct. Eval.* 30 (2011) 186–200.
- [4] Z.Q. Su, L. Ye, Y. Lu, Guided Lamb waves for identification of damage in composite structures: a review, *J. Sound Vib.* 295 (2006) 753–780.
- [5] J.B. Ihn, F.K. Chang, Detection and monitoring of hidden fatigue crack growth using a built-in piezoelectric sensor/actuator network: I. Diagnostics, *Smart Mater. Struct.* 13 (2004) 609–620.
- [6] J.W. Xiang, M. Liang, Multiple damage detection method for beams based on multi-scale elements using Hermite cubic spline wavelet, *Comput. Model. Eng. Sci.* 73 (2011) 267–298.
- [7] J.W. Xiang, M. Liang, A two-step approach to multi-damage detection for plate structures, *Eng. Fract. Mech.* 91 (2012) 73–86.
- [8] H. Sohn, G. Park, J.R. Wait, et al., Wavelet-based active sensing for delamination detection in composite structures, *Smart Mater. Struct.* 13 (2004) 153–160.
- [9] X.T. Miao, D. Wang, L. Ye, et al., Identification of dual notches based on time-reversal Lamb waves and a damage diagnostic imaging algorithm, *J. Intell. Mater. Syst. Struct.* 22 (2011) 1983–1992.
- [10] L. Qiu, M.L. Liu, X.L. Qing, S.F. Yuan, A quantitative multi-damage monitoring method for large-scale complex composite, *Struct. Health Monit.* 12 (2013) 183–196.
- [11] J. Cai, L.H. Shi, S.F. Yuan, et al., High spatial resolution imaging for structural health monitoring based on virtual time reversal, *Smart Mater. Struct.* 20 (2011) 055018.
- [12] L.Y. Yu, V. Giurgiutiu, Multi-damage detection with embedded ultrasonic structural radar algorithm using piezoelectric wafer active sensors through advanced signal processing, *Health Monitoring and Smart NDE of Structural and Biological Systems Conference*, 5768–48, 2005.
- [13] A.S. Purekar, D.J. Pines, S. Sundararaman, et al., Directional piezoelectric phased array filters for detecting damage in isotropic plates, *Smart Mater. Struct.* 13 (2004) 838–850.
- [14] Y. Wang, S.F. Yuan, L. Qiu, Improved wavelet-based spatial filter of damage imaging method on composite structures, *Chin. J. Aeronaut.* 24 (2011) 665–672.
- [15] R.O. Schmidt, Multiple emitter location and signal parameter estimation, *IEEE Trans. Antennas Propag. AP-34* (1986) 276–280.
- [16] Y.B. Fan, F.S. Gu, B. Andrew, Acoustic emission monitoring of mechanical seals using MUSIC algorithm based on higher order statistics, *Key Eng. Mater.* 413–414 (2009) 811–816.
- [17] M. Engholm, T. Stepinski, Direction of arrival estimation of Lamb waves using circular arrays, *Struct. Health Monit.* 10 (2010) 467–480.
- [18] H.J. Yang, Y.J. Lee, S.K. Lee, Impact source localization in plate utilizing multiple signal classification, *Proc. Inst. Mech. Eng., Part C: J. Mech. Eng. Sci.* (2012), <http://dx.doi.org/10.1177/0954406212452233>.
- [19] N. Hu, T. Shimomukai, H. Fukunaga, Z.Q. Su, Damage identification of metallic structures using A_0 mode of Lamb waves, *Struct. Health Monit.* 7 (2008) 271–285.
- [20] V. Giurgiutiu, *Structural Health Monitoring with Piezoelectric Wafer Active Sensors*, vol. 534, Academic Press Inc., Burlington, USA, 2007.
- [21] J.E. Evans, D.F. Sun, J.R. Johnson, Application of Advanced Signal Processing Techniques to Angle of Arrival Estimation in ATC Navigation and Surveillance System, M.I.T. Lincoln Lab, Lexington, MA, 1982, pp. 383.
- [22] T.J. Shan, M. Wax, T. Kailath, On spatial smoothing for direction of arrival estimation of coherent signals, *IEEE Trans. Acoust., Speech Signal Process. ASSP-33* (1985) 806–811.
- [23] S.U. Pillai, B.H. Kwon, Forward/backward spatial smoothing techniques for coherent signal identification, *IEEE Trans. Acoust., Speech Signal Process.* 37 (1989) 8–15.
- [24] L. Qiu, S.F. Yuan, X.Y. Zhang, et al., A time reversal focusing based impact imaging method and its evaluation on complex composite structure, *Smart Mater. Struct.* 20 (2011) 105014.

- [25] M.O.W. Richardson, M.J. Wisheart, Review of low velocity impact properties of composite materials, *Composite Part A 27A* (1996) 1123–1131.
- [26] J.B. Ihn, F.K. Chang, Pitch-catch active sensing methods in structural health monitoring for aircraft structures, *Struct. Health Monit.* 7 (1) (2008) 5–19.
- [27] C.H. Wang, F.K. Chang, Scattering of plate waves by a cylindrical inhomogeneity, *J. Sound Vib.* 282 (2005) 429–459.
- [28] L. Qiu, S.F. Yuan, On development of a multi-channel PZT array scanning system and its evaluating application on UAV wing box, *Sens. Actuators A: Phys.* 151 (2009) 220–230.

Biographies



Yongteng Zhong received his B.S. degree (2007) from Wuhan University of Science and Engineering, and M.S. degree (2010) from Guilin University of Electronic Technology. He is currently working towards the Ph.D. degree at Nanjing University of Aeronautics and Astronautics. His main research interests are low-velocity impact monitoring, structural damage monitoring, and sensor array technology, etc.



Shenfang Yuan received her B.S. (1990), M.S. (1993) and Ph.D. (1996) degree from Nanjing University of Aeronautics and Astronautics. Now she is a professor and the vice director of the Aeronautics Key Lab for Smart Materials & Structures in Nanjing University of Aeronautics and Astronautics. Her main research interests are smart materials and structures, signal processing, intelligent monitoring and intelligent wireless sensor network, etc.



Lei Qiu received his B.S. (2006) and Ph.D. (2012) degree from Nanjing University of Aeronautics and Astronautics. Now he is a lecturer in Nanjing University of Aeronautics and Astronautics. His main research interests are test instrument, sensor technology, signal processing and engineering applications of structural health monitoring, etc.